A fluid description for the discharge equilibrium of a divergent electron cyclotron resonance plasma source

G. Guan and M. E. Mauel
Department of Applied Physics, Columbia University, New York, New York 10027

W. M. Holber and J. B. O. Caughman[a)]
IBM Research Division, T. J. Watson Research Center, Yorktown Heights, New York 10598

(Received 18 March 1992; accepted 2 September 1992)

A fluid description of the presheath of a magnetized plasma is used to model a divergent electron cyclotron resonance (ECR) plasma source. The fluid equations are moments of the time-independent Boltzman equation when cross-field particle motion occurs only through a static $\mathbf{E}\times\mathbf{B}$ drift. Closure is obtained by neglecting third-order moments. The electrons are assumed to have constant temperature along the magnetic field, to obey a Maxwell–Boltzmann potential-density relationship, and to be warmer than the ions. Interactions between plasma and neutral gas are included by specifying the profile of the gas density along the magnetic field and collision cross sections. A form of the equations is derived that can be used to study ions with anisotropic temperatures. The model is used to estimate the axial profiles of the density, ion flow, and ion temperature of an ECR plasma source. The calculated global relationships between (1) the electron temperature and the equilibrium neutral gas density, and (2) the absorbed microwave power and the equilibrium plasma density are comparable with experimental measurements. Furthermore, the calculated ion temperature is comparable to recently reported measurements [Appl. Phys. Lett. **57**, 661 (1990) and Appl. Phys. Lett. **58**, 458 (1991)].

I. INTRODUCTION

Since the introduction of microwave plasma sources that make use of electron cyclotron resonance heating (ECRH) to etch fine-line patterns on semiconductors,[1,2] several experimental investigations have characterized the operation of ECR plasma sources. These studies have documented (1) variations of the plasma density and potential with changes in neutral gas pressure and microwave power,[3–6] (2) the role of magnetic field gradients[7] and magnetic field topology,[8] and (3) the conditions leading to anisotropic etching.[9] More recently, the importance of controlling the ion impact energy was demonstrated by optimizing the plasma etch process through the application of a radio frequency (rf) bias to the substrate surface. The plasma etch rate was enhanced,[10] and etch selectivity was achieved.[11] In addition, measurements of the energy and temperature of the plasma ions and neutral atoms have been made with spectrographic[12] and laser-induced fluorescence (LIF) diagnostics.[13–15] The LIF measurements are noteworthy since they show the perpendicular ion thermal energy to be relatively small ($T_\perp \lesssim 0.5$ eV) and consistent with the observation of anisotropic etching.

In this article, we describe a relatively simple fluid model for the discharge equilibrium of a divergent ECR plasma source. We further show that equilibria calculated with the model resemble many aspects of actual ECR source measurements. The model is an extension of the fluid equations for the plasma presheath developed by Scheuer and Emmert[16] modified to include an axial variation of an applied magnetic field. By construction, kinetic effects are not included, but these effects should be small in an ECR source. For instance, Chodura has shown that a "magnetic presheath" occurs when the magnetic field is oblique to the plasma–wall boundaries,[17] but the magnetic field in most ECR sources is nearly perpendicular to the boundaries. The conduction of ion perpendicular and parallel thermal energy (represented by the higher-order moments of the ion distribution) is also lost in our fluid treatment, but conduction was shown to be small in Ref. 16, especially when $T_e \gg T_i$ as found in ECR sources. Finally, Sato and co-workers[18] have performed a fully kinetic treatment of the collisionless magnetized presheath, but we note that the potential drop and flux reduction which they show results from the flux expansion of a divergent magnetic field is also calculated by the fluid model presented here.

The fluid description of an ECR source can be used to estimate the source's global operating parameters and to calculate the axial profiles of the parallel $T_\parallel$ and perpendicular $T_\perp$ ion "temperatures" along a magnetic field line. For the ions, we use the word "temperature" to refer to a moment of the ion distribution function, but we do not imply that the ions are characterized by a Maxwellian or bi-Maxwellian. On the other hand, we do assume that the plasma electrons are represented by a Maxwell–Boltzmann distribution with a constant temperature T_e and we explain when this approximation is reasonable. By making use of estimates for the power loss due to line radiation,[19] the rates of collisions between plasma and neutrals,[20] and the Pastukhov formula for the total magnitude of the plasma potential,[21,22] we show that the fluid model (1) reproduces the recent LIF measurements of the ion temperature of an

[a)]Present address: Fusion Energy Division, Oak Ridge National Laboratory, Oak Ridge, Tennessee 37831.

 0899-8213/92/124177-10$04.00

ECR source, and (2) reasonably predicts the microwave power and neutral gas density required to achieve a particular plasma density n and electron temperature in an ECR source.

Section II presents the equilibrium fluid equations for the density, parallel flow, and kinetic energy of the plasma ions. These equations describe the steady flow of plasma along both directions of a magnetic field line to perfectly absorbing sheath boundaries. Differential equations for the perpendicular and parallel ion temperatures are derived by finding the moment of the product of the collisional Boltzmann equation and the perpendicular ion kinetic energy. These equations reduce to those presented in Ref. 16 when the axial variation of an applied magnetic field vanishes. Section II also describes the numerical procedure used to solve the fluid equations. Because a plasma discharge has an equilibrium relationship between the electron temperature and the neutral gas density[23] and because the axial magnetic field is not symmetric, the magnitude of gas density and the location of the point of stagnant ion flow are not known *a priori*. This difficulty is overcome by numerical iteration. A unique solution for the discharge equilibrium is found by simultaneously adjusting the magnitude of the neutral gas density and the location of stagnancy until the Bohm sheath criterion is satisfied at both boundaries.

In Sec. III, sample solutions of the equations are presented by modeling the discharge equilibrium of the ECR source used in Refs. 4, 11, and 12. Solutions to the collisionless equations ($T_\perp \neq T_\parallel$) are compared to those obtained when ion collisions are assumed to be sufficiently rapid to insure $T_\perp \approx T_\parallel$. In addition, the equilibrium relation between T_e and the neutral gas density is calculated and compared with experimental measurements obtained using a Langmuir probe. In Sec. IV, the total microwave power required to maintain the discharge is calculated and this relationship is also compared with experimental measurements. Using the model, we are able to illustrate the relative magnitudes of the various power loss channels. A discussion of the implications of this model for optimizing an ECR source is provided in Sec. V.

II. FLUID EQUATIONS FOR THE PRESHEATH IN A MAGNETIZED PLASMA

A. Basic assumptions

In this section, we derive a set of differential equations describing the equilibrium flow of plasma along a magnetic field line typically found in a divergent-field ECR source. These equations will be used later to model the steady-state situation depicted in Fig. 1. Electromagnetic waves are launched through a vacuum window, and the waves propagate along the magnetic field to the electron cyclotron resonance where the plasma electrons are heated. The heated electrons ionize a continuous flow of neutral gas. Once ionized, the plasma ions are assumed to flow along the magnetic field to one of the sheaths, either at the microwave window or at the process surface. An auxiliary magnet is sometimes used to adjust the field strength at the

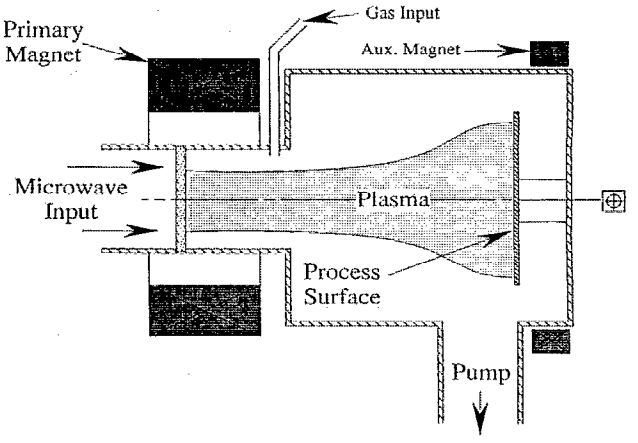

FIG. 1. A schematic drawing of a divergent ECR source illustrating the locations of the quartz window, process surface, and gas feed ring. An auxiliary magnet is sometimes used to adjust the axial magnetic field profile at the process surface.

process surface. We further assume that the materials at both ends of the field line are nonconducting so that the ion and electron flow is ambipolar. For simplicity, cross-field transport is ignored, although a "rotational" $\mathbf{E}\times\mathbf{B}$ drift of electrons and ions V_E is included since the difference in the speeds of the ions and the (stationary) neutral gas is a source of heat to the ions. Magnetic drifts could also be included, but, since the radial gradient scale length of the electrostatic potential is usually much shorter than the radius of curvature of the magnetic field lines, the magnetic drifts are much smaller than V_E. As suggested in Fig. 1, we have in mind a source which is approximately axisymmetric having electron and ion distributions that are constant in the direction of the azimuthal $\mathbf{E}\times\mathbf{B}$ rotation.

Generally, the electron temperature T_e in an ECR plasma source is much larger than both the ion and neutral gas temperatures. Since the electrons are much less massive than the ions, a positive electrostatic potential forms within the plasma to accelerate ions to the sheaths (i.e., the presheath) to maintain ambipolarity. Typically, an electron bounces nearly $\sqrt{M_i/m_e} \sim 500$ times between the sheath boundaries before escaping from the electrostatic well. Furthermore, the electrons are fast enough that the mean-free path for electron energy loss, proportional to $L\sqrt{M_i/m_e}(nT_eC_s/P_\mu)$, is many times the distance between sheaths, $L \sim 50$ cm (see Sec. IV). (In other words, the average electron transit frequency is much less than the electron cooling rate.) For this reason, the average electron energy should be approximately constant along a field line.

In contrast, electron pitch-angle scattering is more frequent. ECR sources usually operate with neutral gas pressures near 1 mTorr, with plasma densities near 10^{12} cm^{-3}, and with electron temperatures near 7 eV. Under these conditions, the mean-free path for electron–electron and elastic electron–neutral collisions is of the order or slightly less than L. Since the electron collision rates are nearly two orders of magnitude larger than electron loss rates, it is reasonable to assume the electrons are well thermalized

having a Maxwellian distribution with temperature T_e. ECRH in magnetic mirrors has been observed to produce non-Maxwellian electrons,[24] but in a divergent-field ECR source, anisotropic, energetic electron tails are not confined. Thus for these reasons and those stated in the previous paragraph, we assume in our calculations that T_e is approximately constant along a field line. In fact, comparisons of the electron temperature measured at the high magnetic field region and at the low field region of ECR plasma sources support this assumption (see Refs. 4 and 5).

The assumption of a Maxwellian electron distribution is very important. The relationship between the electron density and the electrostatic potential becomes local and characterized by the simple relationship

$$\frac{e}{M_i}\frac{\partial \varphi}{\partial s}=\frac{kT_e}{M_i}\frac{\partial \ln n}{\partial s}. \tag{1}$$

In addition, the details of microwave absorption and electron heating can be ignored. (For example, the fact that the electrons may be heated at the Doppler-shifted cyclotron resonance, and at a magnetic field higher than 875 G for 2.45 GHz microwaves, does not enter the plasma power balance.) The absorbed microwave power enters the presheath problem only as a source of energy needed to maintain the given value of T_e.

The coupling between the neutral gas and the plasma is complex in general. For reasons of simplicity, the approach used here is to assume that the neutral gas density along a field line has the form

$$n_0(s)=\tilde{n}_0\, h(s), \tag{2}$$

where $\tilde{n}_0$ is a constant to be determined by the boundary conditions and $h(s)$ is a predefined function of the distance along a field line s. This assumption could be replaced with a self-consistent calculation of the neutral gas density taking into account the gas feed and pumps, but this requires a coupled, two-specie, plasma-gas approach that was not pursued in this analysis.

B. Basic equations

With these assumptions, the procedure for deriving the fluid equations for the presheath described by Scheuer and Emmert (Ref. 16) can be applied directly. The equilibrium Boltzmann equation for the ion distribution is

$$v_\parallel\frac{\partial f}{\partial s}-\left(\frac{e}{M_i}\frac{\partial \varphi}{\partial s}+\frac{\mu}{M_i}\frac{\partial B}{\partial s}\right)\frac{\partial f}{\partial v_\parallel}=\left.\frac{\partial f}{\partial t}\right|_{\rm col}+S, \tag{3}$$

where $v_\parallel$ is the component of velocity parallel to the magnetic field (defined by $v_\parallel=\hat{\mathbf{b}}\cdot\mathbf{v}$), s is the measure of distance along the field line, φ is the electrostatic potential, M_i is the ion mass, $\mu=v_\perp^2 M_i/2B$, $\partial f/\partial t|_{\rm col}$ represents the change of f due to collisions, and S is a particle source. Note that any function of the total energy $E=v^2M_i/2+e\varphi$ is a solution to Eq. (3) in the special case when $\partial f/\partial t|_{\rm col}=S=0$. An arbitrary equilibrium $\mathbf{E}\times\mathbf{B}$ drift, $\mathbf{V}_E=(\mathbf{E}\times\mathbf{B})/B^2$ can also be included in Eq. (3), but, since we have assumed that the distribution is constant around a drift surface at each s, V_E only appears as a relative velocity between the plasma and neutral gas.

Expressing the distribution function in terms of the coordinates $(s,v_\parallel,\mu)$, three moments of Eq. (3) can be found for the density, parallel momentum, and the kinetic energy. Defining the moment $[\![\cdots]\!]$ and average $\langle\cdots\rangle$ operators as

$$[\![...]\!]=\int dv_\parallel\, d\mu\, B(s)... \tag{4}$$

and

$$\langle\cdots\rangle\equiv[\,1/n(s)\,][\![f(s,v_\parallel,\mu)...]\!], \tag{5}$$

we have $\langle\mathbf{v}\rangle=\mathbf{V}_E+V_b$, $\langle v_\perp^2\rangle=V_E^2+2\langle\mu\rangle B/M_i$, and $\langle v^2\rangle=\langle v_\perp^2\rangle+V^2+\langle u_\parallel^2\rangle$.

Atomic and collisional effects are included in the moments of the right-hand side of Eq. (3). The moments of S are represented by the cross sections for ionization σ_i and charge exchange $\sigma_{\rm cx}$ reactions,

$$[\![S]\!]=S_i=nn_0\langle\sigma_i v\rangle_e, \tag{6}$$

$$[\![v_\parallel S]\!]=-S_{\rm co}V=-nn_0\sigma_{\rm cx}\bar{V}V, \tag{7}$$

$$[\![v^2S]\!]=(S_i+S_{\rm cx})(3kT_s/M_i+2V_E^2)-\langle v^2\rangle S_{\rm cx}, \tag{8}$$

$$\left[\!\!\left[\left(V_E^2+\frac{2\mu B}{M_i}\right)S\right]\!\!\right]=(S_i+S_{\rm cx})\left(\frac{2kT_s}{M_i}+2V_E^2\right)-\langle v_\perp^2\rangle S_{\rm cx}. \tag{9}$$

Here, S_i is the ionization source rate, $S_{\rm cx}$ is the charge-exchange rate, the root-mean-square speed of the ions with respect to the neutrals is approximated by $\bar{V}=\langle v^2\rangle^{1/2}$, and T_s is the temperature of the source particles. In Eqs. (8) and (9), the average energy of an ion immediately following ionization or charge exchange from a neutral atom is assumed to be $1.5\,kT_s+M_iV_E^2$ (i.e., the sum of the average energy of the neutral gas and the energy resulting from acceleration by the radial electric field). Elastic scattering from neutrals is modeled with a "smooth" sphere model (Ref. 20) and denoted by the cross section σ_0. For Coulomb collisions, we use the formula used by Spitzer,[25] and denote the characteristic electron Coulomb collision time as τ_e, and the ion–ion Coulomb collision time as τ_i. This gives

$$\left[\!\!\left[\left.\frac{\partial f}{\partial t}\right|_{\rm col}\right]\!\!\right]=0, \tag{10}$$

$$\left[\!\!\left[v_\parallel\left.\frac{\partial f}{\partial t}\right|_{\rm col}\right]\!\!\right]=-R_0V, \tag{11}$$

$$\left[\!\!\left[\frac{1}{2}v^2\left.\frac{\partial f}{\partial t}\right|_{\rm col}\right]\!\!\right]=Q_i-R_0\Delta E_0, \tag{12}$$

$$\left[\left(\frac{1}{2}V_E^2+\frac{\mu B}{M_i}\right)\frac{\partial f}{\partial t}\bigg|_{\rm col}\right]$$

$$=Q_{i,\perp}-R_0\left[\Delta E_{0,\perp}-\frac{1}{12}\left(V^2-V_E^2+\langle u_\parallel^2\rangle-\frac{\langle\mu\rangle B}{M_i}\right)\right]. \tag{13}$$

Here, Q_i represents energy transferred due to Coulomb collisions, and R_0 represents elastic scattering. The average total and perpendicular energy lost to the neutrals from the streaming ions per collision are denoted by ΔE_0 and $\Delta E_{0,\perp}$, respectively. The definitions of the moments in Eqs. (10)–(13) are taken to be the expressions

$$R_0=nn_0\sigma_0\overline{V}, \tag{14}$$

$$Q_i=\frac{m_e n}{M_i\tau_e}\left(\frac{3kT_e}{M_i}-\langle u_\parallel^2\rangle-\frac{2\langle\mu\rangle B}{M_i}\right), \tag{15}$$

$$Q_{i,\perp}=\frac{2}{3}Q_i+\frac{n}{\tau_i}\left(\langle u_\parallel^2\rangle-\frac{\langle\mu\rangle B}{M_i}\right), \tag{16}$$

$$2\Delta E_0\approx\frac{1}{2}\langle v^2\rangle-\frac{3kT_s}{2M_i}, \tag{17}$$

$$2\Delta E_{0,\perp}\approx\frac{1}{2}\langle v_\perp^2\rangle-\frac{kT_s}{M_i}. \tag{18}$$

Making use of these definitions, the three moment equations become

$$B\frac{\partial}{\partial s}\left(\frac{nV}{B}\right)=S_i, \tag{19}$$

$$B\frac{\partial}{\partial s}\left(\frac{n}{B}(V^2+\langle u_\parallel^2\rangle)\right)=-\frac{en}{M_i}\frac{\partial\varphi}{\partial s}-\frac{n\langle\mu\rangle}{M_i}\frac{\partial B}{\partial s}-V(R_0+S_{\rm cx}), \tag{20}$$

$$B\frac{\partial}{\partial s}\left[\frac{nV}{2B}\left(V^2+V_E^2+3\langle u_\parallel^2\rangle+\frac{2\langle\mu\rangle B}{M_i}\right)+\frac{n}{2B}\left(\langle u_\parallel^3\rangle+\frac{2\langle u_\parallel\mu\rangle B}{M_i}\right)\right]$$
$$=-nV\frac{\partial}{\partial s}\left(\frac{e\varphi}{M_i}-\frac{1}{2}V_E^2\right)+Q_i+\frac{3kT_s}{2M_i}S_i+(S_i+S_{\rm cx})V_E^2-\Delta E_0(2S_{\rm cx}+R_0). \tag{21}$$

Equations (19)–(21) reduce to Eqs. (2) and (3) of Ref. 16 when $S_{\rm cx}=R_0=Q_i=V_E=\partial B/\partial s=0$.

Closure of the moment hierarchy requires expressions for $\langle u_\parallel^3\rangle$ and $\langle u_\parallel\mu\rangle$. These terms represent the conduction of parallel and perpendicular ion thermal energy. As previously mentioned, these third-order moments can be justifiably ignored whenever $T_e\gg T_i$. Indeed, even when $T_e\sim T_i$, Scheuer and Emmert (Ref. 16) have shown heat conduction contributes only about 10% of the total heat flux to the sheath in an unmagnetized plasma.

The fluid equations can be applied in two cases. The "collisional" case corresponds to conditions when pitch-angle scattering is sufficient to ensure that $\langle u_\parallel^2\rangle\approx\langle\mu\rangle B/M_i\approx kT/M_i$. The "collisionless" case corresponds to conditions when $\langle u_\parallel^2\rangle\equiv kT_\parallel/M_i\neq kT_\perp\equiv\langle\mu^2\rangle B$. In the following two subsections, we present first-order equations for $\partial n/\partial s$, $\partial V/\partial s$, and $\partial T/\partial s$ for these two cases.

C. Fluid equations with drifting, isotropic ions

The fluid equations for a collisional, isotropic plasma are found when defining $\langle u_\parallel^2\rangle\approx\langle\mu\rangle B/M_i\approx kT/M_i$. In this case, the moment equations become

$$\frac{\partial n}{\partial s}=\frac{-1}{V(C_s^2-V^2)}\left(\frac{2}{3}Q_0+S_iV^2+nV^3\frac{\partial\ln B}{\partial s}\right), \tag{22}$$

$$\frac{\partial V}{\partial s}=\frac{1}{n(C_s^2-V^2)}\left(\frac{2}{3}Q_0+S_iC_s^2+nVC_s^2\frac{\partial\ln B}{\partial s}\right), \tag{23}$$

$$\frac{\partial T_i}{\partial s}=\frac{(M_i/k)}{nV(C_s^2-V^2)}\left[\left(C_s^2-V^2-\frac{2kT_i}{3M_i}\right)\times\left(\frac{2}{3}Q_0-(S_i+S_{\rm cx}+R_0)V^2\right)-V^2\frac{2kT_i}{3M_i}\times\left(2S_i+S_{\rm cx}+R_0+nV\frac{\partial\ln B}{\partial s}\right)\right], \tag{24}$$

where we have defined a net ion heating density Q_0 as

$$Q_0\equiv Q_i+(S_i+S_{\rm cx}+R_0)\left(2V^2+\frac{1}{2}V_E^2-\frac{3k}{2M_i}(T_i-T_s)\right)-S_i\frac{kT_i}{M_i}+\frac{1}{4}R_0\left(V^2-3V_E^2+\frac{3k}{M_i}(T_i-T_s)\right).$$

In the collisional equations, the sound speed is defined to be $C_s^2\equiv k(T_e+5T_i/3)/M_i$. The average squared ion velocity is $\langle v^2\rangle=V^2+V_E^2+3kT_i/M_i$.

Notice that the fluid equations are singular as $|V|\to C_s$ and as $V\to 0$. The singularity when the flow becomes sonic corresponds to the location of the electrostatic Debye sheath, and this singularity is forced to occur at a sheath boundary by adjusting the neutral gas density. As shown in Ref. 16, the singularity at the stagnation point $V(s^*)=0$ is removed by an appropriate choice of T_i [i.e., $Q_0(s^*)=0$]. This requires the ion temperature to be

$$\frac{kT_i(s^*)}{M_i}=\frac{2Q_i+3(kT_s/M_i)(S_i+S_{\rm cx}+\frac{1}{2}R_0)+V_E^2(S_i+S_{\rm cx}-\frac{1}{2}R_0)}{5S_i+3S_{\rm cx}+\frac{3}{2}R_0}. \tag{25}$$

At $s=s^*$, we assign $n(s^*)=n^*$. Equations (22)–(24) indicate $dn/ds=dT_i/ds=0$ at s^*. Notice, that since V is small at s^*, S_{cx}, and R_0 are small compared to S_i, and $kT_i(s^*)\sim 3kT_s/5+M_i(2Q_i/S_i+V_E^2)/5$. Since T_s is small in ECR sources, even a modest radial electric field usually dominates central ion heating, and $kT_i(s^*)\sim M_iV_E^2/5$.

D. Fluid equations with drifting, anisotropic ions

When collisions are infrequent compared with the ion transit time from the plasma source, the ion distribution will not be a drifting Maxwellian. In this case, separate equations for $\partial T_\parallel/\partial s$ and $\partial T_\perp/\partial s$ can be constructed. First, the moment of Eq. (3) with $\mu B/M_i+V_E^2/2$ is found, and, then, this equation is subtracted from Eq. (21) in order to find the equation for the conservation of parallel energy. The moment of the perpendicular energy is

$$B\frac{\partial}{\partial s}\left[\frac{nV}{B}\left(\frac{V_E^2}{2}+\frac{\langle\mu\rangle B}{M_i}\right)\right]$$
$$=nV\left[\frac{\partial}{\partial s}\left(\frac{1}{2}V_E^2\right)+\frac{\langle\mu\rangle B}{M_i}\frac{\partial \ln B}{\partial s}\right]-(R_0+2S_{cx})\Delta E_{0,\perp}$$
$$+Q_{i,\perp}+\frac{kT_s}{M_i}S_i+V_E^2(S_i+S_{cx})-\frac{1}{12}R_0$$
$$\times\left(V^2-V_E^2+\langle u_\parallel^2\rangle-\frac{\langle\mu\rangle B}{M_i}\right), \tag{26}$$

and the equation for the axial variation of the parallel energy is

$$B\frac{\partial}{\partial s}\left(\frac{nV}{2B}(V^2+3\langle u_\parallel^2\rangle)\right)$$
$$=-nV\left(\frac{e}{M_i}\frac{\partial\varphi}{\partial s}+\frac{\langle\mu\rangle B}{M_i}\frac{\partial \ln B}{\partial s}\right)+(Q_i-Q_{i,\perp})+\frac{kT_s}{2M_i}S_i$$
$$-(\Delta E_0-\Delta E_{0,\perp})(2S_{cx}+R_0)+\frac{1}{12}R_0$$
$$\times\left(V^2-V_E^2+\langle u_\parallel^2\rangle-\frac{\langle\mu\rangle B}{M_i}\right). \tag{27}$$

Equations (19), (20), (26), and (27) can now be rewritten as coupled nonlinear equations for the equilibrium profiles of n, V, $\langle u_\parallel^2\rangle\equiv kT_\parallel/M_i$, and $\langle\mu^2\rangle B\equiv kT_\perp$. These equations are

$$\frac{\partial n}{\partial s}=\frac{-1}{V(C_s^2-V^2)}\left[2Q_0+S_iV^2+nV\right.$$
$$\left.\times\left(V^2+\frac{k}{M_i}(T_\perp-3T_\parallel)\right)\frac{\partial \ln B}{\partial s}\right], \tag{28}$$

$$\frac{\partial V}{\partial s}=\frac{1}{n(C_s^2-V^2)}\left[2Q_0+S_iC_s^2+nV\right.$$
$$\left.\times\left(C_s^2+\frac{k}{M_i}(T_\perp-3T_\parallel)\right)\frac{\partial \ln B}{\partial s}\right], \tag{29}$$

$$\frac{\partial T_\parallel}{\partial s}=\frac{(M_i/k)}{nV(C_s^2-V^2)}\left\{\left(C_s^2-V^2-\frac{2kT_\parallel}{M_i}\right)[2Q_0-V^2(S_i\right.$$
$$+S_{cx}+R_0)]-2\frac{kT_\parallel}{M_i}\left[V^2(2S_i+S_{cx}+R_0)\right.$$
$$\left.\left.+nV\left(C_s^2+\frac{k}{M_i}(T_\perp-3T_\parallel)\right)\frac{\partial \ln B}{\partial s}\right]\right\}, \tag{30}$$

$$\frac{\partial T_\perp}{\partial s}=\frac{(M_i/k)}{nV}\left[Q_\perp+(S_i+S_{cx}+R_0)\left(\frac{V_E^2}{2}-\frac{k}{M_i}(T_\perp\right.\right.$$
$$\left.-T_s)\right)+\frac{1}{6}R_0\left(\frac{1}{2}V^2-5V_E^2+\frac{3k}{M_i}(T_\perp-T_s)\right.$$
$$\left.\left.-\frac{k}{2M_i}(T_\perp-T_\parallel)\right)+nV\frac{kT_\perp}{M_i}\frac{\partial \ln B}{\partial s}\right], \tag{31}$$

where, for these equations, Q_0 is defined as

$$Q_0\equiv(Q_i-Q_\perp)+(S_i+S_{cx}+R_0)\left(V^2-\frac{k}{2M_i}(T_\parallel-T_s)\right)$$
$$-S_i\frac{kT_\parallel}{M_i}+\frac{1}{12}R_0\left(2V^2+V_E^2+\frac{3k}{M_i}(T_\parallel-T_s)\right.$$
$$\left.+\frac{k}{M_i}(T_\perp-T_\parallel)\right).$$

In the collisionless case, the sound speed is $C_s^2\equiv k(T_e+3T_\parallel)/M_i$, and the average square velocity is $\langle v^2\rangle=V^2+V_E^2+k(T_\parallel+2T_\perp)/M_i$.

As was the case for the collisional equations, the singularity at $V=0$ is removed by choosing appropriate values of $T_\parallel$ and $T_\perp$ at the stagnation point. Since $Q_\perp\propto(T_\parallel-T_\perp)$, this requires the simultaneous solution of Eqs. (30) and (31) as $V\to 0$. At the point of stagnancy, $n(s^*)=n^*$, $V=0$, and

$$\frac{kT_\parallel(s^*)}{M_i}=\frac{2(Q_i-Q_\perp)+(R_0/6)(T_\perp-T_\parallel)+(kT_s/M_i)(S_i+S_{cx}+R_0/2)+\frac{1}{6}V_E^2R_0}{3S_i+S_{cx}+(R_0/2)},$$
$$\frac{kT_\perp(s^*)}{M_i}=\frac{Q_\perp-(R_0/12)(T_\perp-T_\parallel)+(kT_s/M_i)(S_i+S_{cx}+R_0/2)+(V_E^2/2)(S_i+S_{cx}-\frac{2}{3}R_0)}{S_i+S_{cx}+(R_0/2)}. \tag{32}$$

In the collisionless equations, the temperature and density profiles have a finite axial gradient at the stagnancy point due to the $\mu\,\partial B/\partial s$ force,

$$\left.\frac{\partial n}{\partial s}\right|_{s^*} = -n^* \frac{k(T_\perp - 3T_\parallel)}{M_i C_s^2} \frac{\partial \ln B}{\partial s},$$

$$\left.\frac{\partial T_\parallel}{\partial s}\right|_{s^*} = -2T_\parallel \left(1 + \frac{k(T_\perp - 3T_\parallel)}{M_i C_s^2}\right) \frac{\partial \ln B}{\partial s}, \qquad (33)$$

$$\left.\frac{\partial T_\perp}{\partial s}\right|_{s^*} = T_\perp \frac{\partial \ln B}{\partial s}.$$

The central ion temperatures in the collisionless case are approximately $kT_\parallel \sim kT_s/3 + 2M_i(Q_i - Q_\perp)/3S_i$ and $kT_\perp \sim kT_s + M_i(Q_\perp/S_i + V_E^2/2)$. When $kT_s < M_i V_E^2/2$, $T_\perp > T_\parallel$ at $s = s^*$.

III. EXAMPLE EQUILIBRIUM OF AN ECR PLASMA SOURCE

A. Numerical solution technique

In practice, both the collisional and collisionless fluid equations are difficult to solve because of the complex geometry of an ECR source. The nonuniform magnetic field and the nonuniform neutral gas density prevents the use of symmetry arguments to identify the location of the stagnation point s^* where $V = 0$. Furthermore, for a given discharge length (defined as $L = s_2 - s_1$ with the quartz window located at s_1 and the process surface at s_2), the requirement that $|V| \to C_s$ at both sheath boundaries defines an equilibrium condition between the electron temperature and the neutral gas profile. If Eq. (19) is integrated, then

$$\left.\frac{nC_s}{B}\right|_{s=s_1}^{s=s_2} = \int_{s_1}^{s_2} \frac{ds}{B} n n_0 \langle \sigma_i \nu \rangle_e, \qquad (34)$$

and the generic equilibrium scaling between T_e and n_0, $n_0 \sim C_s/L\langle \sigma_i \nu \rangle_e$, is clearly illustrated. However, in a magnetic field, we have noticed that unusual neutral gas and magnetic field profiles may prevent satisfying simultaneously the Bohm sheath criterion at both boundaries. For instance, if dB/ds is sufficiently negative, dV/ds may also become negative when the decrease in density due to the expansion of the plasma's flux tube exceeds a critical ionization rate. In this case, a steady-state flow equilibrium could not be found. However, for all of the profiles which we will discuss here, a discharge equilibrium always exists for any given value of T_e provided the profile of the neutral gas density is properly normalized.

The "collisional" equations [Eqs. (22)–(24)] or the "collisionless" equations [Eqs. (28)–(31)] can be solved for given values of T_e and peak density $n(s^*) = n^*$ using well-known integration schemes.[26] A single integration determines the axial locations at which $|V| \to C_s$. In general, this will not correspond to the actual sheath locations (i.e., s_1 and s_2) so new choices of the neutral density $n_0(s) = \tilde{n}_0 h(s)$ and stagnation point s^* are repeatedly chosen until sonic flow occurs at both sheath boundaries. Since we have prescribed an axial profile of the neutral gas [Eq. (2)], an equilibrium is identified uniquely by the values of $\tilde{n}_0$ and s^*. With this iteration scheme, a solution with accuracy of one part in 10^4 could be obtained on a personal computer in approximately 2 min.

B. Example solution

Figure 2 illustrates a solution to the collisional fluid equations for a typical operating condition of the ECR plasma source described in Refs. 4, 11, and 12. The quartz window was located at $s_1 = 10$ cm, and the electrically isolated stainless steel substrate was located at $s_2 = 72$ cm. In order to best represent the actual operating conditions of the source, the peak density n^* and electron temperature corresponded to those measured with a Langmuir probe that was inserted from the side of the vacuum chamber to the axis at $s = 44$ cm. The probe characteristics were analyzed using standard methods.[27] For the example in Fig. 2, the injected microwave power was 1500 W; the operating gas was argon; the gas flow rate was 50 sccm; and the probe measurements were $T_e \approx 6.1$ eV and $n^* \approx 0.79 \times 10^{12}$ cm^{-3}. The gas feed ring was located at $s = 30$ cm, and a high capacity vacuum pump was located behind the substrate. The argon pressure in the source could only be measured in the absence of the plasma, and, for this example, the initial argon fill pressure was 1 mTorr. When the microwave power was switched on, a steady, uniform plasma was generated with a diameter of approximately 20–25 cm at $s = 44$ cm.

Figure 2(a) shows the "inputs" used in the fluid equilibrium calculation. The magnetic field strength along the central field line of the source $B(s)$ and the assumed axial profile of the neutral gas density $h(s)$ are shown. This particular neutral profile was selected (1) to represent the rapid pumping of the plasma due to ionization and the gas recycling at the window and the substrate, and (2) to place the stagnancy point between the quartz window and the gas feed ring, $s_1 = 10$ cm $< s^* < 30$ cm. This later condition insures that the axial acceleration of the ions created near the gas ring is directed to the pump, $s > s_2 = 72$ cm. The neutral argon temperature was assumed to be 580 K (Ref. 15), and, for this density, the atoms had a mean-free path for ionization of approximately 9 cm. No direct measurement of V_E was available so, for this example, V_E was taken arbitrarily to be $0.3\sqrt{kT_e/M_i}$.

Figure 2(b) shows the axial profiles of the calculated equilibrium profiles, $n(s)$, $V(s)$, and $T_i(s)$ (i.e., the "outputs"). The magnitude of the presheath is calculated to be approximately $0.8\,kT_e/e$, and kT_i increase from 0.15 eV at the stagnation point to 0.35 eV at the sheaths. The argon density was calculated to be 5×10^{12} cm^{-3} ($\sim$0.3 mTorr) at the process surface but only 0.8×10^{12} cm^{-3} within the plasma.

C. Ion temperature profile using the collisionless fluid equations

The equilibrium profiles of an ECR source computed with the collisionless fluid equations are similar to those

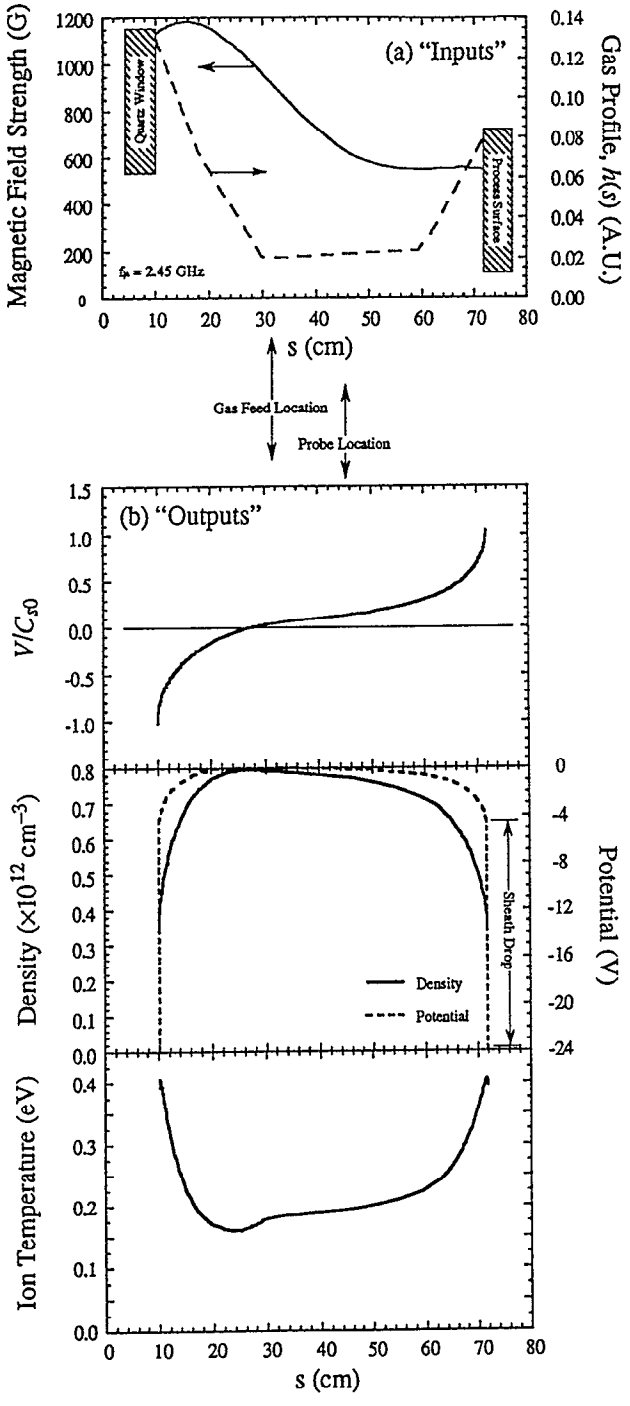

FIG. 2. An example solution of the equilibrium discharge parameters along a magnetic field line. This solution corresponds to operation of the source in Refs. 4, 11, and 12, with 50 sccm argon gas and 1500 W of microwave power. The electron temperature measured with the probe and used in the simulation was 6.1 eV. (a) The assumed magnetic field and neutral gas profiles, and (b) the calculated flow, ion density, potential, and temperature profiles.

shown in Fig. 2 except at low plasma density. When the source is operated at low plasma density, ion–ion collisions are sufficiently weak to allow $T_{\|} \neq T_{\perp}$. (Remember, in this context, we do not imply that f is a Maxwellian or bi-Maxwellian distribution, instead we use the term "temperature" only to represent a moment of the ion distribution.)

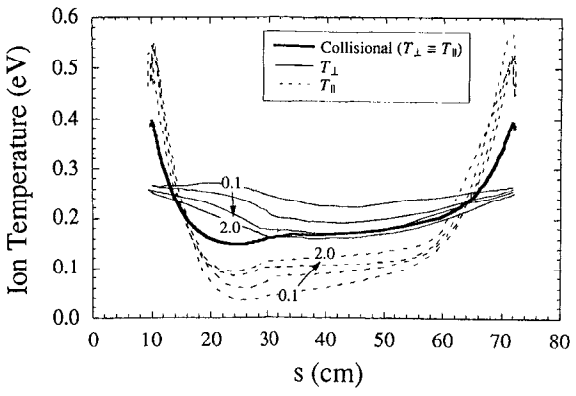

FIG. 3. The variation of the parallel (---) and perpendicular (——) ion temperatures along the magnetic field. The four "collisionless" solutions correspond to plasma densities of $n^*=0.1$, 0.5, 1.0, and 2.0×10^{10} cm^{-3}. The heavy solid line is the collisional solution with $n^*=4.5\times10^{11}$ cm^{-3}. These "temperatures" represent the axial variation of moments of the ion distribution function.

Figure 3 illustrates the ECR equilibria calculated using the collisionless equations. The solutions were obtained using the same geometry as before although lower power operation with 0.9 kW of microwave power, 40 sccm of argon, and $T_e=5.9$ eV was simulated. In order to illustrate significant temperature anisotropy, the plasma density at the stagnation point was reduced to $n^*=0.1$, 0.5, 1.0, and 2.0×10^{10} cm^{-3}. These low-density equilibria are compared to the solution of the collisional equations when n^* was set to the measured value of 0.45×10^{12} cm^{-3}. Since the electron temperature was constant for each example, the peak argon neutral density and the location of the stagnancy point (required to match both sheath boundary conditions) did not significantly change.

Figure 3 is a significant result. It illustrates the mechanisms for ion heating in an ECR source, and it shows that the equilibria calculated from the fluid equations predict ion temperatures of the same magnitude as recent LIF measurements (Refs. 13–15). As shown in Eq. (31), near the stagnation point, the parallel temperature is determined primarily by the gas temperature ($T_s\sim0.05$ eV), while the perpendicular temperature is determined by a combination of the gas temperature and the radial electric field. This results in $T_{\perp} > T_{\|}$ near $s=s^*$. As the ions accelerate to the sheaths, the axial flow of the ions relative to the neutrals approaches C_s, and ionization and charge-exchange significantly broaden the parallel ion distribution. This heating effect produces $T_{\|} > T_{\perp}$ within about 8 cm of the sheath boundaries, and this mechanism is probably most responsible for ion heating. Since V_E^2 and C_s^2 are both proportional to T_e, we find that the magnitude of T_i scales linearly with T_e. This trend was also seen experimentally by Den Hartog and co-workers (Ref. 13). As the collisionless solutions show, even with the highest plasma density tested, the ionization of neutrals when the ion flow is nearly sonic (i.e., at the sheath boundaries) produces very anisotropic ion distributions. This is consistent with measurements made by Trevor and co-workers (Ref. 14).

In fact, they noted that the parallel ion distribution may become bimodal a few centimeters from the substrate when the neutral pressure is low and T_e and C_s are high.

D. The equilibrium relation between T_e and $\tilde{n}_0$

To illustrate the equilibrium relationship between the electron temperature and the neutral gas pressure in an ECR plasma source, we have calculated equilibria corresponding to a wide range of plasma source operation. Langmuir probe measurements of n^* and T_e were made as the microwave power was increased from 0.3 to 1.5 kW and the argon flow rate was increased from 15 to 50 sccm. Then, the discharge equilibrium was found from the fluid equations for each of the measured operating points. For simplicity, we assumed in our calculations that the neutral gas profile was fixed even as conditions changed. The profile $h(s)$ shown in Fig. 2(a) was used for all simulations. This approximation is probably the least satisfactory in our study since the measured n^* varied from 10^{11} cm^{-3} to 8×10^{11} cm^{-3}, significantly changing the mean-free path for ionization of the argon gas. Nevertheless, even when $h(s)$ is held constant, we still find the calculated equilibrium relationship resembles the relationship between neutral density and electron temperature measured experimentally.

The results of the calculation are shown in Fig. 4. The open boxes represent the calculated argon pressure at 580 K at the boundary of the plasma as the electron temperature increases from 4.5 to 9.0 eV. Since the gas profile was fixed, the calculated equilibria follow the single relationship, P=4 mTorr ($C_s/L\langle\sigma_i v\rangle_e/3.5\times10^{13}$ cm^{-3}). The prefill pressure of argon (measured at room temperature prior to switching on the microwave power) is also shown in Fig. 4 although the data are plotted using a vertical scale 3.8 times larger than the scale used to plot the calculated pressures. The measured relationship between T_e and n_0 is seen to generally follow the same trend as calculated with the equilibrium fluid equations. To operate with high T_e, low gas pressure is required, and low T_e operation requires higher gas pressure. It is important to emphasize that for a fixed neutral gas profile, the relationship between T_e and n_0 is independent of the microwave power and plasma density. On the other hand, the gas profile is not constant in an actual ECR source. The left-to-right horizontal scatter in the measured points represent the increase in microwave power at fixed flow rate. As the microwave power increases, the plasma density also increases, reducing the argon mean-free path for ionization. For this reason, the neutral profile $h(s)$ should change as the power increases, and this slightly modifies the experimentally measured equilibrium relationship between T_e and n_0.

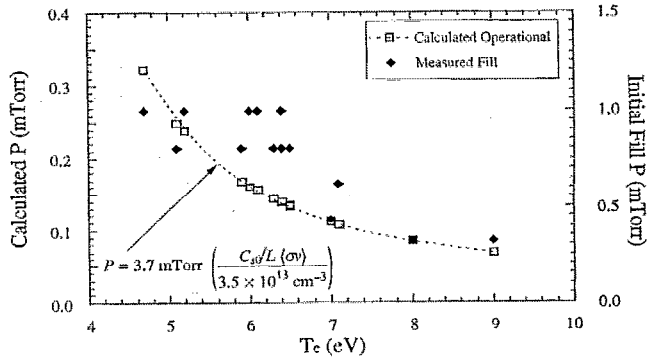

FIG. 4. The measured and calculated relationship between the electron temperature and the neutral gas density. For the experiment, only measurements of the argon flow rate and initial fill pressure were available.

IV. MICROWAVE POWER BALANCE

Once the equilibrium profiles for an ECR source have been calculated, the microwave power required to maintain the plasma flow can be estimated. The microwave power is absorbed by the electrons at the resonant magnetic field B_r. As explained in Ref. 8, this input power balances (1) the flow of particle energy along the field line to the sheath boundaries, (2) the heating of neutral gas through charge transfer and elastic collisions, and (3) the ionization and excitation of neutrals from electron impact collisions with neutrals. Since we have assumed that the plasma and microwave power flux is uniform along an $\mathbf{E}\times\mathbf{B}$ drift surface, the equilibrium cross-field rotation does not enter the power balance equation. In this case, the microwave power flux P_μ absorbed at the resonant magnetic field required to maintain the discharge equilibrium is

$$P_\mu=\sum_{i=1,2}\frac{B_r}{B(s_i)}\left[nC_s\left(\frac{1}{2}M_i(C_s^2+V_E^2)+\frac{3}{2}kT_\parallel+kT_\perp+\frac{\alpha_e kT_e}{1-\gamma_e}+e\Delta\Phi_s\right)\right]_i+B_r\int_{s_1}^{s_2}\frac{ds}{B}\left[S_i\left(\chi_i-\frac{3}{2}kT_s\right)\right.$$
$$\left.+(2S_{cx}+R_0)\Delta E_0+p_r\right]+\left[\sum_{i=1,2}\left(\frac{B_r}{B(s_i)}nC_s e\Phi(s^*)\right)_i-B_r\int_{s_1}^{s_2}\frac{ds}{B}S_i e\Phi(s)\right], \tag{35}$$

where we have made use of Eq. (21). Equation (35) gives the power balance for a particular flux tube. The first term on the right-hand side of Eq. (35) represents the sum of the ion and electron energy flux absorbed at the two endwalls (i.e., at $s=s_1$ and s_2). The term $\Delta\Phi_s$ represents the acceleration of ions across the electrostatic Debye sheath. The emission of secondary electrons at the sheaths has the coefficient γ_e. In order to estimate the size of $\Delta\Phi_s$, we calculated the total size of the electrostatic potential required for ambipolar electron loss using the bounce-

averaged Pastukhov formalism presented in Ref. 22 and including the effects of secondary electron emission. The boundary in electron velocity-space separating trapped and lost electrons is an ellipsoidal surface with a parallel radius equal to $\sqrt{2e\Phi^*/m_e}$. Pastukhov's formula adjusts the size of this boundary so that the collisional current of electrons from the trapped region of velocity space to the untrapped region equals the sum of the ion flux to both sheath boundaries. Both electron–electron and elastic electron–neutral collisions were used to calculate this rate. Enhancement of the electron loss due to electron cyclotron resonance heating (Ref. 24) was ignored. The term α_e was taken to be $2B(s_i)/[B_r+B(s_i)]$, reflecting the reduction of the electron kinetic energy lost to the walls as the trapped-region in velocity space becomes spherical [i.e., as the mirror-ratio, $B(s_i)/B_r$ vanishes]. The second term in Eq. (35) is the integral of the ionization losses (χ_i is the energy required for ionization), charge-exchange and elastic ion–neutral scattering losses (proportional to ΔE_0), and line radiation density p_r. In order to estimate the magnitude of the line radiation, the approximation given in Ref. 19 was used. Griem's approximation is appropriate when resonant transitions to the ground state dominate and when the density is sufficiently small that excitation from multiple inelastic electrons collisions are infrequent. The third and last term of Eq. (35) represents the power required to heat the electrons created from ionization to an energy sufficient to escape from the ambipolar potential barrier. As described in Ref. 22, this term reflects the fact that electrons born through ionization within the plasma have initially a negative potential energy with repect to the boundary surfaces.

For the discharge in Fig. 2, the power required to supply the ionization, radiation, and charge-exchange losses [i.e., the second term of Eq. (35)] contributed 57% of the total power required to sustain the equilibrium. The ion and electron power lost to the substrate [i.e., the first term of Eq. (35)] was 27% of the total, and that lost to the window was 12.5% of the total power absorbed. The remaining 3.5% of the power was required to heat the electrons over their confining potential [i.e., the third term of Eq. (35)]. A figure of merit for ECR plasma sources is the power required per amp equivalent of ion flux to the substrate. For the discharge in Fig. 2, this figure of merit was 183 W/A. This number is not equivalent to the ratio of the total microwave power and the total particle current to the substrate since it does not account for power absorbed on field lines that intersect vacuum chamber walls or other radial variations of parameters.

Probably the most important feature of Eq. (35) is the nearly linear relationship between the plasma density and the required power flux. Figure 5 illustrates this relationship by plotting the power required to sustain the equilibria as a function of the density measured by the Langmuir probe. The calculated power flux scales approximately as $P_\mu \approx 5$ W/cm^2 ($n/10^{12}$ cm^{-3}). The small deviation from linear scaling results from the variation in the gas density which causes a variation in the electron temperature. The actual microwave power injected into the plasma source is also presented in Fig. 5 (plotted with a different vertical

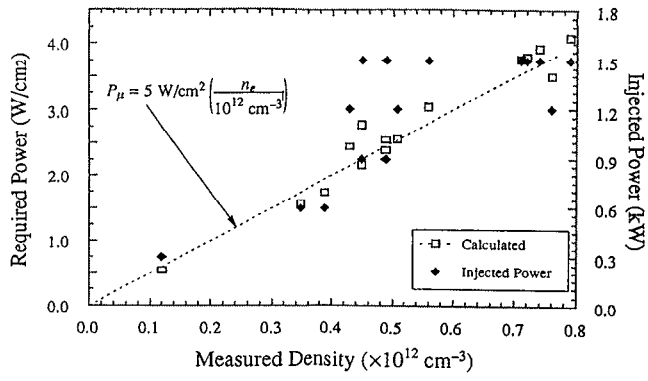

FIG. 5. The measured and calculated relationship between the absorbed microwave power flux and the plasma density.

scale). As was the case in Fig. 4, the experimentally observed relationship between the injected power and the plasma density resembles that calculated with the equilibrium fluid equations. The horizontal scatter of the experimental points occurs as the argon flow rate is adjusted at fixed power. Low flow rates produce high electron temperatures and this is seen to increase slightly the power required to sustain a given plasma density.

Figure 5 is significant because the absolute magnitude of the required power calculated from Eq. (35) is comparable to measurements even without the use of any adjustable parameters. Since the plasma diameter was measured to be approximately 20 cm at $s=44$ cm, we can estimate an average flux of absorbed microwave power. Assuming uniform microwave illumination of the plasma, the actual injected power P_{inj} divided by the measured plasma cross section gives approximately 4.3 W/cm^2 (P_{inj}/1 kW) absorbed at the resonance zone. As can be seen from Fig. 5, this average power flux is about 1.5 times larger than the power flux calculated from the discharge equilibrium. If the microwave power was absorbed on the central field lines with 66% efficiency, then the calculated and the measured power-density relationship would be identical. We believe that it is not unreasonable that up to one-third of the injected microwave power can be absorbed at the edge of the plasma where field lines intersect the vacuum chamber wall and (to a lesser extent) within the source cavity walls or microwave tuners. Indeed, the close agreement between Eq. (35) and the measured power-density relationship over a wide operating range illustrates the usefulness of the fluid equations to understand and predict the operation of ECR plasma sources.

V. DISCUSSION

In this article, we have shown the equilibrium fluid equations generalized from those presented in Ref. 16 can be used to estimate the profiles of the plasma density, ion flow speed, and ion "temperature" along any particular field line of a divergent ECR source. The equations also illustrate the primary mechanism for ion heating. The ion temperature near the point of stagnancy is determined by the magnitude of V_E and, generally, $T_\perp > T_\parallel$. As the ion

flow becomes sonic, the relative speed between the neutral gas and the ions increase, and ionization near the sheath boundaries increases the parallel ion temperature. The fluid equations also allow calculation of the equilibrium relationship between the electron temperature and the neutral gas density. We find that the measured (T_e, n_0) relationship to be comparable to that predicted with the fluid calculations although the evolution of the neutral gas profile $h(s)$ as the microwave power increases has not yet been evaluated. In addition, we find the radiation and ionization losses dominate the microwave power required to maintain the discharge, and a simple formula, containing no adjustable parameters, can reasonably approximate actual ECR source power requirements.

The results presented here suggest how the operation of an ECR plasma source will change as its size and configuration changes. For example, we have examined the equilibrium of commercially available plasma sources (such as the S1000 or S1500 devices from Applied Science and Technology, ASTeX). These sources were used for the measurements reported in Refs. 13–15. The ASTeX sources have a slightly shorter length between window and process surface and a much larger ratio of magnetic field strengths $B_r/B(s_1)$ than the source described in Fig. 2. The smaller magnetic field at the substrate widens the magnetic flux tube and reduces the plasma density and particle flux nC_s at this location. Both the presheath drop and the length along which the plasma flows near sonic speeds increase in the ASTeX source. This causes the ion temperature to double relative to that shown in Fig. 2, exceeding 0.7 eV at the process surface.

The fluid equations for an ECR plasma source can also suggest ways to optimize the ECR plasma source. For instance (without considering details of microwave coupling to the plasma), the effective ion temperature at the substrate can be reduced by shortening the source length L and adjusting the ratio of the magnetic field strengths $B_r/B(s_1)$ to be near unity. A shorter source length decreases T_e for a given neutral pressure [see Eq. (27)], and the high field at the substrate minimizes power requirements. Conversely, when T_e increases, the fraction of absorbed power radiated will reduce while the power incident to the process surface will increase. It seems reasonable to us that a variety of possible ECR plasma source configurations could be simulated with the technique described in this article. Also, process gases other than argon can be simulated provided that the appropriate atomic cross sections were known.

Finally, we believe the results presented here motivate several further areas of study. The fluid equations for the plasma equilibrium should be combined with an atomic transport code in order to determine $h(s)$ self-consistently. Detailed measurements of the actual equilibrium profiles are needed so that local instead of global comparisons can be made between theory and experiment. In addition, the assumption of Maxwellian electrons with a single temperature needs to be examined both experimentally and computationally. In particular, energetic electron effects arising from mirror trapping in a nonmonotonic magnetic field profile could be simulated using a Fokker–Planck calculation.[28]

ACKNOWLEDGMENTS

The authors wish to acknowledge many useful discussions with Dr. J. Forster.

This work was supported by a grant from the IBM Corporation and National Science Foundation Grant No. ECS 89-12756.

[1] K. Suzuki, S. Okudaira, N. Sakudo, and I. Kanomata, Jpn. J. Appl. Phys. **16**, 1979 (1977).
[2] K. Suzuki, K. Ninomiya, and S. Nishimatsu, Vacuum **34**, 953 (1984).
[3] J. Musil, Vacuum **36**, 169 (1986).
[4] J. Forster and W. Holber, J. Vac. Sci. Technol. A **7**, 899 (1989).
[5] O. A. Popov, J. Vac. Sci. Technol. A **7**, 894 (1989).
[6] S. M. Gorbatkin, L. A. Berry, and J. B. Roberto, J. Vac. Sci. Technol. A **8**, 2893 (1990).
[7] M. Matsuoka and K. Ono, J. Vac. Sci. Technol A **6**, 1987 (1988).
[8] J. Asmussen, J. Vac. Sci. Technol. A **7**, 883 (1989).
[9] Y. Tobinaga, N. Hayashi, H. Araki, and S. Nakayama, J. Vac. Sci. Technol. B **6**, 272 (1988).
[10] K. Suzuki, K. Ninomiya, S. Nishimatsu, and S. Okudaira, J. Vac. Sci. Technol. B **3**, 1025 (1985).
[11] W. M. Holber and J. Forster, J. Vac. Sci. Technol. A **8**, 3720 (1990).
[12] J. S. McKillop, J. C. Forster, and W. H. Holber, Appl. Phys. Lett. **55**, 30 (1989).
[13] E. A. Den Hartog, H. Persing, and R. C. Woods, Appl. Phys. Lett. **57**, 661 (1990).
[14] D. J. Trevor, N. Sadeghi, T. Nakano, J. Derouard, R. A. Gottscho, P. D. Foo, and J. M. Foo, Appl. Phys. Lett. **57**, 1188 (1990).
[15] T. Nakano, N. Sadeghi, and R. A. Gottscho, Appl. Phys. Lett. **58**, 458 (1991).
[16] J. T. Scheuer and G. A. Emmert, Phys. Fluids B **2**, 445 (1990).
[17] R. Chodura, Phys. Fluids **25**, 1628 (1982).
[18] K. Sato, F. Miyawaki, and W. Fukui, Phys. Fluids B **1**, 725 (1989).
[19] H. R. Griem, *Plasma Spectroscopy* (Academic, New York, 1966).
[20] E. W. McDaniel, *Collision Phenomena in Ionized Gases* (Wiley, New York, 1964).
[21] V. P. Pastukhov, Nucl. Fusion **14**, 3 (1976).
[22] R. H. Cohen, M. E. Rensink, T. A. Cutler, A. A. Mirin, Nucl. Fusion **18**, 1229 (1978).
[23] A. von Engel, *Ionized Gases* (Oxford U.P., London, 1965).
[24] M. E. Mauel, Phys. Fluids **27**, 12 (1984).
[25] L. Spitzer, Jr., *Physics of Fully Ionized Gases* (Wiley, New York, 1962).
[26] See, for example, W. H. Press, B. P. Flannery, S. A. Teukolsky, and W. T. Vetterling, *Numerical Recipes* (Cambridge U.P., Cambridge, 1986).
[27] I. H. Hutchinson, *Principles of Plasma Diagnostics* (Cambridge U.P., Cambridge, 1990).
[28] Y. Matsuda and J. J. Stewart, J. Comput. Phys. **66**, 197 (1986).